# Portable Relative Humidity Sensor Using Agarose-Coated Polymer Optical Fibers

MD Shahadat Hossain, Weiyang Xu, Laraib Unsa Noor, Muhammad Saleh Urf Kumail Haider, Abdul Ghaffar, Zain Ul Abdin, Farooque Ahmed, MD Bipu Arman, and Chen Chen, *Senior Member, IEEE*

Abstract—**This work presents a compact smartphone-integrated relative humidity (RH) sensor based on intensity modulation using agarose-coated polymer optical fibers (POFs). The sensing architecture employs a tapered, twisted-coupling configuration of dual POFs to maximize evanescent-field interaction with the surrounding medium. Coating the coupling region with a thin hygroscopic agarose layer imparts substantial humidity-dependent optical loss, enabling sensitive and reversible RH detection. Utilizing the smartphone's integrated flashlight as the light source and its camera as the photodetector, this system establishes a portable, cost-effective, and instrument-free measurement platform. The RH sensor demonstrates a linear response over a broad RH range, 20–90% RH, with a sensitivity of 0.117 μW/%RH measured using a laboratory power meter and a normalised intensity responsivity of 0.106%/%RH under smartphone readout. The portable RH sensor provides a resolution of approximately 0.12$\pm$0.01%RH and maintains excellent repeatability across multiple cycles. These features support practical RH monitoring in settings where conventional optical instrumentation is impractical or unavailable.**

Index Terms—**Relative humidity, polymer optical fiber (POF), coupling, agarose gel, portable sensor.**
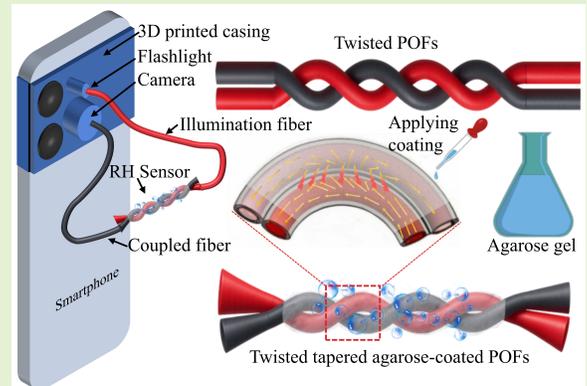
I. Introduction

HUMIDITY is a key parameter in environmental monitoring and plays an essential role across industrial production, healthcare, and the preservation of cultural heritage. For example, in semiconductor processing, pharmaceutical storage, food packaging, and smart building management, it is essential to measure relative humidity (RH) accurately to make sure that products are safe, reliable, and of high quality [1, 2]. Conventional electronic humidity sensors typically based on capacitive, resistive, or thermal conductivity mechanisms are widely used due to their technological maturity [3]. Nev-

ertheless, their performance can be constrained by susceptibility to electromagnetic interference, drift over time, limited sensitivity in harsh environments, and the need for regular recalibration, which restricts their use in certain demanding conditions.

Several optical fiber RH sensors have been reported, utilizing the variety of fiber geometries designs, coating materials and modes of interrogation [4, 5]. For example, the most widely used designs includes fiber Bragg gratings (FBG) [6], Mach–Zehnder interferometers (MZI) [7], Fabry–Perot interferometers (FPI) [8], and surface plasmon resonance (SPR) techniques are mostly reported for RH sensor fabrication [9]. In the realm of coatings, various materials such as polymers, oxides and 2D materials have been explored for their humidity sensing [5, 10, 11]. Guo et al. [12] proposed an organically modified polymer-coated FBG based RH sensor. Zhang et al. [13] fabricated a pentaerythritol tetra acrylate microcavity with a truncated cone structure. Whereas, Chen et al. [14] reported more advanced 3D-printed FPI castle-style microcavities, which achieved sensitivities up to 248.9 pm/%RH but required costly femtosecond laser based two photon polymerization techniques. Johari et al. [15] improved humidity response using ZnO nanorod-coated tapered U-shaped polymer optical fiber (POF). Furthermore, Fu et al. [16] reported a tapered dual side hole fiber coated with graphene oxide (GO) film, demonstrating fast response and recovery times of 0.23s and 2.19s. However, while coating strategies like

MD Shahadat Hossain, Weiyang Xu, Laraib Unsa Noor, Muhammad Saleh Urf Kumail Haider, MD Bipu Arman, Chen Chen are with the School of Microelectronics and Communication Engineering, Chongqing University, Chongqing 400044, China (e-mail: mdshahadat825969@gmail.com; weiyangxu@cqu.edu.cn; laraib@stu.cqu.edu.cn; haider@stu.cqu.edu.cn; bipuarman@gmail.com; c.chen@cqu.edu.cn).

Abdul Ghaffar is with the College of Mechanical Engineering, Quzhou University, Quzhou 32400, Zhejiang, China (e-mail: ghaffar@qzc.edu.cn).

Zain Ul abdin and Farooque Ahmed are with the Department of Electronics, Faculty of Engineering and Technology, University of Sindh, Jamshoro, 76080, Pakistan (e-mail: zainulabdeen927@gmail.com; farooquebrohi1999@gmail.com).

GO, ZnO nanorods, and microcavities enhance sensitivity, they raise concerns regarding long-term stability, environmental durability, and scalability [11].

Hydrogel-based sensors have attracted significant research attention for their exceptional properties, including high water-absorption capacity, customizable mechanical properties, and excellent biocompatibility [17]. For instance, Xia et al. [18] used a poly N-isopropylacrylamide hydrogel-based FPI with response and recovery times of 2.29 s and 1.90 s, respectively. Hu et al. [19] developed a microstructured POF with gold agarose coating to take advantage of SPR and achieved the sensitivity of 0.595 μW/%RH of 20% and 80% RH. Tong et al. [20] also combined SPR and MZI in a single structure, using a modified optical fiber coated with graphene quantum dots and polyvinyl alcohol (PVA) as the RH-sensitive material. Similarly, Wang et al. [21] created side-polished POF sensor that were coated with PVA thin films up to a sensitivity limit of 10.15 nm/%RH. Although the approaches are highly sensitive, the modulation and fabrication processes are expensive and complicated. Sadam et al. [22] proposed a POF-based intensity-modulated RH sensor with a linear response across the sensing range. An additional work suggested a twisted POF sensor for distributed RH monitoring via fiber coupling [23]. Despite their strong sensing performance, these approaches often remain constrained by limited portability and relatively narrow RH measurement ranges. In response, more recent work has increasingly emphasized RH sensors that are not only highly sensitive but also affordable, durable, and genuinely portable, aiming to extend the operational range while preserving stability under real-world conditions.

As the limitations of conventional optical fiber sensor technologies have become increasingly apparent, the field has moved toward practical, integrated sensing platforms that can deliver reliable measurements without relying on expensive laboratory instrumentation [24-26]. In parallel, sensors embedded in users personal devices most notably smartphones are emerging as a realistic option for environmental monitoring, driven by their ubiquity, accessibility, and steadily advancing capabilities [27, 28]. This shift leverages the integrated computational power, diverse sensor arrays, and robust connectivity of smartphones, thereby enabling real-time data acquisition and analysis across a multitude of environmental parameters. For instance, Haider et al. [29] proposed a smartphone based dual point level sensor to be cost effective and allow users to conduct measurements without specialized laboratory equipment. Another study explores a portable refractive index (RI) sensor using intensity variation techniques with twisted POFs [30]. Despite these advancements, a significant gap remains in the development of highly sensitive, cost-effective, and portable smartphone-integrated RH sensors that offer a wide detection range, thereby overcoming the limitations of both traditional and optical fiber-based methodologies.

In this work, we present a compact humidity sensor based on twisted tapered side-coupled POFs coated with an agarose gel. The technique employs two stripped POFs brought into contact and geometrically twisted to form a coupling region, where one fiber serves as the optical input and the second acts as the output channel for the coupled light. The sensing
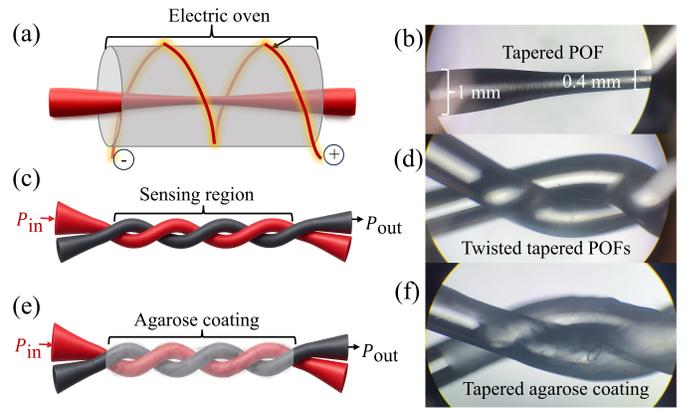

Fig. 1. The complete fabrication process of portable RH sensor. (a) heat oven for tapering, (b) microscopic picture of tapered fiber, (c) twisting of tapered part, (d) microscopic picture of the twisting part, (e) agarose coating and (f) microscopic picture of coated sensing part.

mechanism relies on intensity modulation, where changes in the surrounding medium alter the RI of the agarose-coating, which modifies the optical power coupling. To enable practical deployment, the sensor is interfaced directly with a smartphone by aligning the fiber input with the phone's flashlight as the illumination source and the output with the camera as the photodetector to track humidity-dependent intensity variations. The agarose-coated RH sensor demonstrates portable, high-resolution, and maintains linear operation over a wide RH range of 20%–90%. Overall, integrating smartphone readout with a POF-based sensing architecture offers a low-cost, simple, and high-performance route toward real-time, field-deployable humidity monitoring.

II. Research Methodology

A. Sensor fabrication

The proposed humidity sensor is based on a tapered twisted coupling architecture formed using two bare POFs. Step-index SK-40 fibers were used for fabrication, featuring a 980 μm core diameter and a 20 μm cladding thickness. The RI contrast between the core and cladding ensures efficient light guidance via total internal reflection, while the intrinsic flexibility of POF enables twisting and coupling without structural damage. As summarized in Fig. 1, the fabrication of the portable optical fiber RH sensor comprises three main steps: tapering, coupling, and agarose coating.

1) Tapering: The POFs were tapered by localised heating in an electrically heated oven, followed by controlled pulling as illustrated in Fig. 1(a). As the polymer softens, a gradual waist is formed, reducing the core and cladding dimensions and bringing the evanescent field closer to the surrounding environment. The tapering reduces the POF's diameter to 0.4 mm, as shown in resolution microscopic image of tapered fiber in Fig. 1(b). The 0.4 mm diameter was optimized to maximize coupling efficiency while maintaining mechanical robustness within the twisted side-coupling region. Whereas tapers exceeding this dimension yielded negligible improvements in efficiency, smaller diameters resulted in structural fragility and compromised stability. This process significantly

increases evanescent field penetration and strengthens the interaction between guided light and the ambient medium. The effectiveness of this process can be expressed using the tapering efficiency η_{tap}, which reflects the redistribution of optical power from the core toward the cladding and surrounding material.

2) Coupling: Two tapered POFs, configured as an illumination fiber (IF) and a coupled fiber (CF), are twisted together to form a mechanically stable side-coupling region. Light is launched into the IF as the input power (P_{in}), and a portion of this optical power couples into the CF. Because the coupling region is distributed along the contact length, coupled light can be guided toward both ends of the CF. In our configuration, the forward-propagating end of the CF is selected as the measurement port and is defined as the sensor output (P_{out}).

For repeatable sensor performance, a commercial twisting machine was used to apply a uniform twist density of 2 twists/cm. The twisting-induced coupling behavior is governed by the coupling coefficient η_{tw}, which depends on the twist geometry and determines the stability and consistency of optical power transfer. After tapering and twisting, the structure defines an effective sensing region of 3 cm within the tapered twisted section, where the enhanced evanescent field yields increased sensitivity to humidity-driven refractive index variations.

3) Coating: The twisted sensing region was coated with a 0.5 wt% agarose gel to form an RH-responsive layer with a humidity-dependent RI. The gel was prepared by dissolving agarose powder in deionized water at 50 °C under continuous stirring until the solution became optically clear, then cooling it to a workable temperature before coating. After application the coated fiber was dried for 24 hours.

As RH increases, the agarose absorbs moisture and swells, improving index matching and reducing the effective gap between the tapered fibers, which strengthens coupling from the IF to the CF and increases the transmitted signal [31]. The microscopic images in Fig. 1(d, f) confirm a well-formed taper, uniform twisting, and consistent agarose deposition. This simple fabrication approach enables a compact, low-cost, and sensitive platform for portable humidity sensing.

B. Sensor Theory

The RH sensor consists of two identical POFs which have been tapered to increase the evanescent field and helically twisted against each other in physical contact to a finite length L and uniformly covered with a 0.5 wt% agarose gel. RH leads to absorption of water in agarose and it alters the RI of the gel causing swelling. These changes reduce the microscopic gap between the tapered fibers, improve index matching, and strengthen evanescent field coupling from the IF to the CF. Consequently, the optical power collected at the end of the CF increases with RH as modeled by the coupled-power differential equations [32, 33]:

$$\begin{cases} \dfrac{dP_0}{dx} = -(\alpha_0 + \beta)\,P_0 + \beta\,P_1 \\[2mm] \dfrac{dP_1}{dx} = \beta\,P_0 - (\alpha_1(RH) + \beta)\,P_1 \end{cases} \tag{1}$$

where $x \in [0, L]$ is the coordinate along the coupling region. The optical powers carried by the IF and CF are $P_0(x)$ and $P_1(x)$, respectively. α_0 is the effective attenuation in the IF within the coated tapered zone, $\alpha_1(RH)$ is the RH-dependent attenuation in the CF capturing scattering and index-matching changes, and $\beta(RH)$ is the RH-dependent coupling coefficient length L.

The coupling coefficient rises with humidity because swelling shrinks the inter-fiber gap and improves modal overlap. A parametric form that captures this behavior is:

$$\beta(RH) = \beta_0\,\eta_{\text{tap}}\,\eta_{\text{tw}}\,\exp\!\left(-\frac{d(RH)}{w}\right) \tag{2}$$

where β_0 fixes the coupling scale for dry, uncoated contact, $\eta_{\text{tap}} > 1$ accounts for the larger evanescent fraction created by tapering, η_{tw} summarizes phase matching contact enhancement due to twisting, $d(RH)$ is the mean separation between the two tapered cores inside the agarose. w is an effective evanescent field decay length in the taper. All quantities are constants except $d(RH)$, which increases with humidity. Over the calibration range of 20–90% RH, the gap evolution is well approximated by an affine relationship:

$$d(RH) = d_0 - \gamma\,RH \tag{3}$$

where d_0 is the dry-state mean separation and $\gamma > 0$ is a swelling coefficient determined by the 0.5 wt% agarose composition and the mechanical constraint of the twisted pair. Humidity also reduces loss in the CF by smoothing micro roughness and improving RI matching within the gel. A first-order description suffices for fitting:

$$\alpha_1(RH) = \alpha_{1,\text{dry}} - k_\alpha\,\frac{RH}{100} \tag{4}$$

Here $\alpha_{1,\text{dry}}$ is the CF attenuation in dry conditions and $k_\alpha > 0$ is the net loss-reduction slope (per %RH) that lumps scattering and index effects and implies α_1 decreases linearly with RH over the operating range. The boundary conditions follow single-port excitation at the entrance:

$$P_0(0) = P_{\text{in}}, \qquad P_1(0) = 0 \tag{5}$$

where P_{in} is the launched optical power into the IF at $x = 0$ while the CF carries no power at the start of the coupling region. These conditions match the experimental arrangement where only one fiber is directly illuminated. Solving Eq. (1) subject to the boundary conditions in Eq. (5) for a uniform coupling section of length L yields the following closed-form power distributions:

$$\begin{cases} P_0(x) = \dfrac{P_{\text{in}}}{2}\left(1 + e^{-2\beta(RH)x}\right)e^{-\alpha_0 x} \\[3mm] P_1(x) = \dfrac{P_{\text{in}}}{2}\left(1 - e^{-2\beta(RH)x}\right)e^{-\alpha_1(RH)x} \end{cases} \tag{6}$$

In these expressions the factors $e^{-\alpha_0 x}$ and $e^{-\alpha_1(RH)x}$ represent attenuation along the respective paths, while the terms $(1 \pm e^{-2\beta(RH)x})/2$ encode the progressive exchange of power caused by coupling that accumulates with distance.
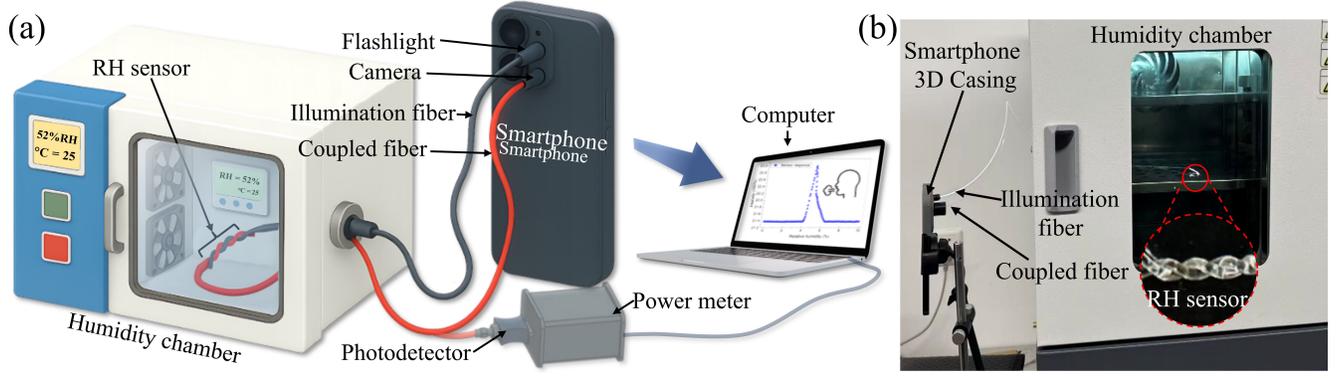
Fig. 2. Portable RH sensor illustration diagram: (a) schematic, and (b) experimental setup picture.

The measurable quantity is the CF power at the exit of the coated region:

$$P_{\text{out}}(RH) = P_1(L) = \frac{P_{\text{in}}}{2}\left(1 - e^{-2\beta(RH)L}\right) e^{-\alpha_1(RH)L} \tag{7}$$

Here, $P_{\text{out}}(RH)$ is the detector-side signal used for RH estimation; it depends on RH only through $\beta(RH)$ from Eqs. (2) and (3) and $\alpha_1(RH)$ from Eq. (4). Because β increases and α_1 decreases with humidity, P_{out} rises monotonically with RH and approaches a gentle plateau when $2\beta(RH)L \gg 1$.

C. Experimental Setup

The experimental arrangement for the proposed portable RH sensor is shown in Fig. 2. The agarose-coated tapered twisted POF pair was placed inside a calibrated environmental chamber to maintain stable and repeatable temperature and humidity conditions. As RH increased, the agarose continuously absorbed moisture and its RI changed, which altered the coupling efficiency between the twisted fibres and produced a corresponding intensity variation at the CF output. Throughout all experiments, the smartphone flashlight served as the only light source for the IF. The coupled output from the CF was recorded either with an optical power meter (Thorlabs PM100USB) with photodetector (Thorlabs S151C), or by the smartphone camera for portable measurements. For the smartphone readout, the built-in LED flashlight was aligned to launch light into the IF, while the rear wide-angle camera captured the intensity emerging from the CF. A custom 3D-printed casing was used to hold the fibres and ensure fixed alignment between the fibre ends, the smartphone flash, and the camera.

To ensure repeatability, the automatic camera functions were held constant throughout each experiment, including exposure, ISO, focus, and white balance. The POFs was secured in a 3D-printed casing to maintain a fixed alignment between the flashlight light and camera sensor. The videos were acquired at 30 fps with a resolution of 1920 × 1080 pixels and processed in MATLAB. For comparison with the theoretical formulation Eq. (9), each video frame was reduced to a single scalar intensity value using a weighted region of interest (ROI) approach and then scaled to a known RH reference. The baseline intensity I_0 was defined as the average ROI

intensity measured at the initial reference humidity (RH_0) after stabilization, while I_{RH} denotes the ROI intensity at a given RH. Each frame was first converted to grayscale to avoid color-channel bias. A circular ROI was defined around the bright spot emitted from the fiber output, and a Gaussian weighting function was applied to emphasize the core signal while suppressing background noise. The frame wise intensity was computed as a weighted spatial average:

$$I_t = \frac{\sum_{(x,y)\in\mathcal{R}} W(x,y)\, G_t(x,y)}{\sum_{(x,y)\in\mathcal{R}} W(x,y)} \tag{9}$$

where $G_t(x,y)$ is the grayscale value (0-255 for 8-bit) at pixel (x,y) in frame t, $\mathcal{R}$ denotes the fixed circular ROI centered on the fiber spot, and the ROI center (x_0,y_0) was selected at the peak-intensity location in the first frame and kept fixed for the entire recording. The weighting function $W(x,y)$ is defined by a Gaussian profile:

$$W(x,y) = \exp\left(-\frac{(x-x_0)^2 + (y-y_0)^2}{2\sigma^2}\right) \tag{10}$$

centered at (x_0,y_0) with width σ chosen to match the optical spot. The RH response was expressed as the normalized differential intensity relative to the baseline: $\Delta I(\%) = \frac{I_{RH}-I_0}{I_0} \times 100\%$, enabling straightforward calibration and real-time monitoring.

III. RESULTS AND DISCUSSION

A. Tapered Coupled POFs

The proposed RH sensor was characterized using both a standard power meter and a smartphone-based measurement platform. The smartphone flashlight served as the sole optical source, the transmitted power was recorded with the optical power meter and smartphone camera. Measurements were performed for twisted–tapered coupled POF structures with and without the agarose coating, and the resulting responses were compared to quantify the contribution of the agarose sensing layer to RH detection.

To isolate the contribution of tapering to RH sensing in a twisted-coupling geometry, we first compared the responses of two configurations using an optical power meter. First, a twisted tapered POF pair; second, a twisted-only untapered POF pair. As shown in Fig. 3(a,b), both humidification and
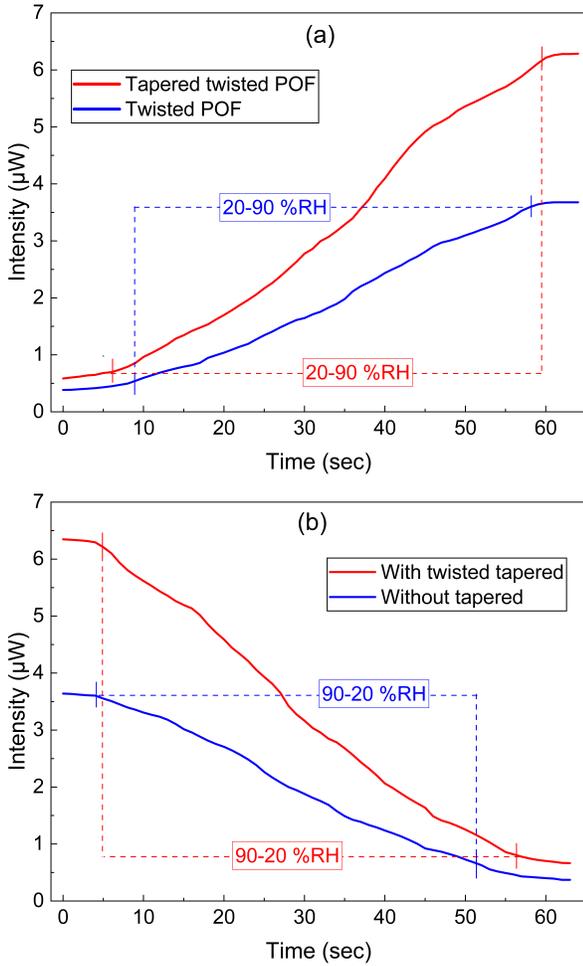
Fig. 3. The response of twisted tapered and untapered sensors while: (a) humidification and (b) dehumidification.

Fig. 4. Twisted tapered coated and uncoated sensor response to humidity variation: (a) humidification, and (b) dehumidification.

dehumidification cycles reveal markedly stronger coupling for the tapered twisted coupled sensor. In humidification, the twisted tapered sensor reaches an output power of approximately 6.3 μW, whereas the untapered sensor only about 3.7 μW. A similar trend is observed during dehumidification, where the twisted tapered structure exhibits a larger intensity change, indicating higher sensitivity to RH variations. These results confirm that combining tapering with twisting enhances light matter interaction by increasing evanescent field penetration and improving coupling efficiency, which together translate into a stronger humidity dependent power modulation.

B. Agarose Coating

Agarose gel is highly hydrophilic and can absorb water from its surroundings, including moisture from the air. When the relative humidity increases, water molecules diffuse into the agarose network through hydration of polar groups, which causes the gel to swell. This swelling changes the local optical environment around the twisted–tapered coupling region by modifying the effective RI and the contact condition between the two coupled POF tapers. As a result, a larger fraction of the radiated optical power interacts with the coating region
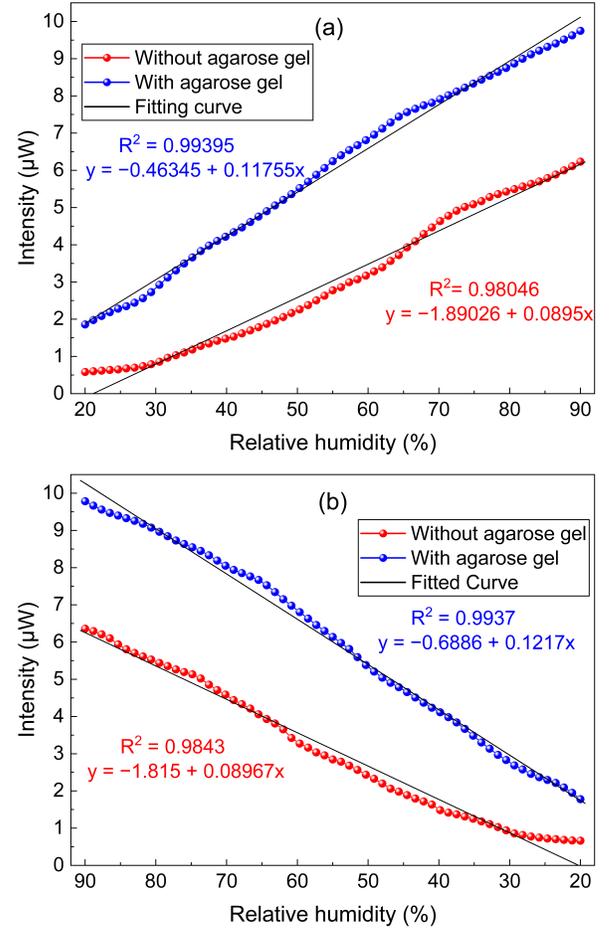
and the coupled power becomes more strongly dependent on humidity.

Fig. 4(a) illustrates the RH response of the twisted tapered sensor with and without the agarose coating. In both sensor configurations, the coupled optical power increases as RH rises. However, the agarose-coated sensor exhibits a markedly steeper response because the hydrogel readily absorbs moisture and swells, shifting its RI and improving the coupling region between the two twisted tapers of POFs. This humidity-driven RI modulation enhances coupling efficiency and produces a more substantial power change with RH. It will lead to a greater sensitivity of 0.117 μW/%RH with a correlation coefficient R^2=0.99395, whereas the uncoated sensor shows a lower slope of 0.089 μW/%RH with R^2=0.98046.Fig. 4(b) shows the dehumidification behaviour of the agarose-coated and uncoated sensor.This improvement is attributed to moisture absorption and swelling of the agarose, which increases interaction between the guided field and the surrounding medium and strengthens the coupling efficiency in the twisted–tapered region.

C. Portable RH Sensor

The proposed RH sensor was further evaluated in a portable configuration using a smartphone, where the built-in flashlight
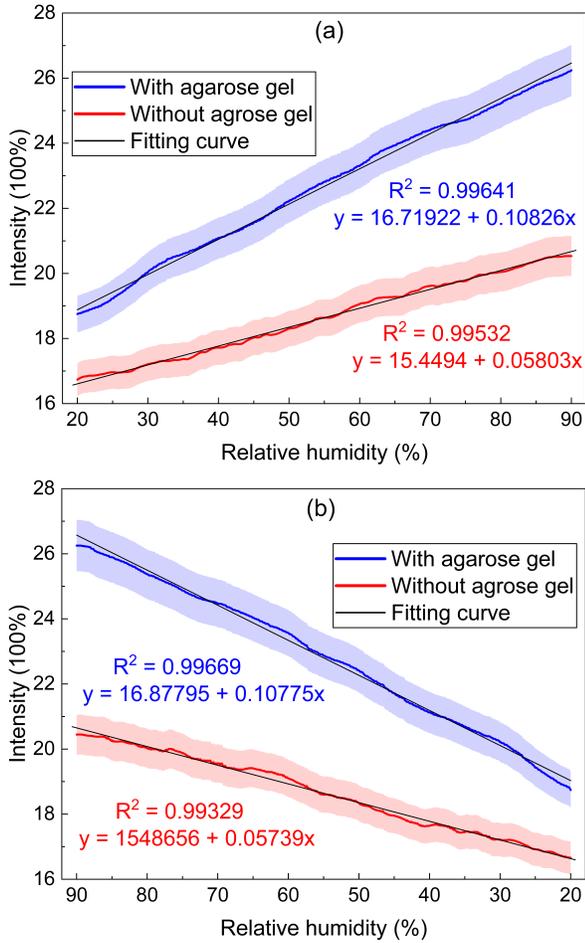
Fig. 5.   Smartphone based readout of agarose coated and uncoated RH sensor during: (a) humidification and (b) dehumidification.

Fig. 6.   Comparison of RH sensing with a power meter and smartphone camera with (a) %RH increase and (b) %RH decrease.

served as the light source and the rear camera recorded humidity induced intensity variations. Fig. 5(a,b) compares the smartphone responses of the twisted tapered POF sensor with and without the agarose coating. Fig. 5(a) illustrates the sensor response during humidification where agarose-coated sensor exhibits stronger power transfer to CF than the uncoated sensor, consistent with enhanced coupling in the presence of the agarose layer, and it achieves a sensitivity of 0.1082%/RH. During dehumidification, the agarose-coated sensor still maintains a sharper response. However, a slight reduction in sensitivity is observed, decreasing to -0.1077%/RH, as shown in Fig. 5(b). Importantly, the smartphone measurements closely reproduce the trends obtained with the optical power meter, validating the interrogation approach and confirming that the coating improves sensitivity. Moreover, the smartphone-based readout provides a practical portable alternative with high resolution RH of $\approx 0.12 \pm 0.01$/%RH, supporting low cost, field-deployable humidity monitoring.

D. Power Meter vs Smartphone Camera Comparison

Fig. 6 compares the RH response by using the optical power meter and the smartphone camera after normalizing both outputs. This compariso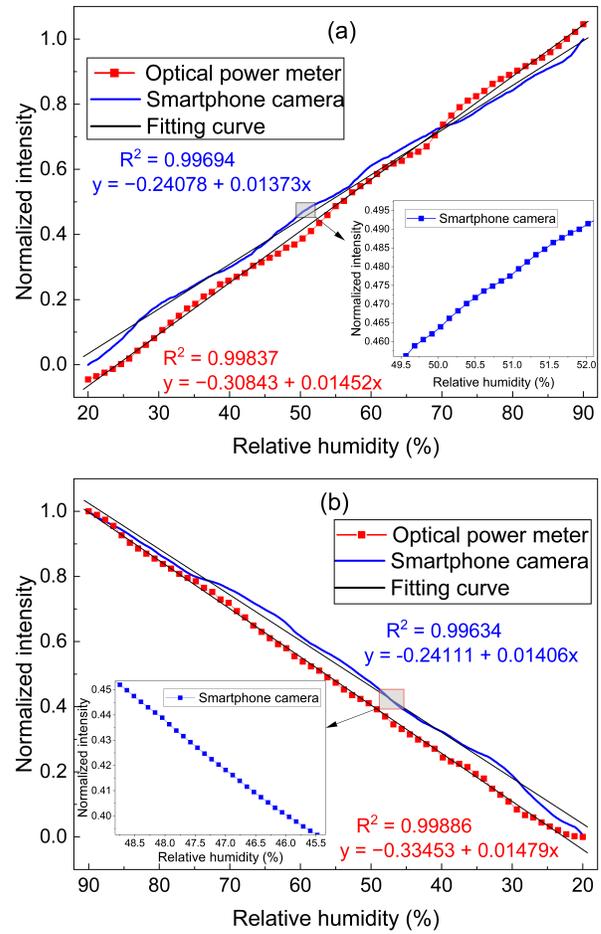n is important because it separates the sensing behaviour of the agarose-coated coupling region from the measurement hardware, and it shows whether the smartphone can reproduce the same humidity-dependent trend measured with laboratory instrumentation. Fig. 6(a) shows a clear rise in normalized intensity as RH increases from 20% to 90%. The power meter data follow a smooth monotonic trend, consistent with stronger evanescent coupling as the agarose absorbs moisture, swells, and undergoes a humidity dependent RI shift, giving a high linear fit $R^2 = 0.99837$. The smartphone readout closely tracks the same behavior, with only small deviations, which indicates that grayscale intensity extracted from the camera frames is sufficiently sensitive to resolve the incremental changes in coupled optical power $R^2 = 0.99694$. During dehumidification Fig. 6(b), the response reverses as expected the normalized intensity decreases as the coating dehydrates and coupling weakens, and the smartphone curve again follows the power meter measurements across the full range with strong linearity $R^2 = 0.99886$ for the power meter and $R^2 = 0.99634$ for the smartphone.

The slight differences between the power meter and smartphone results are expected because the two detectors collect and process light differently. The power meter measures total incident power, while the smartphone camera records an image-based intensity that depends on factors such as
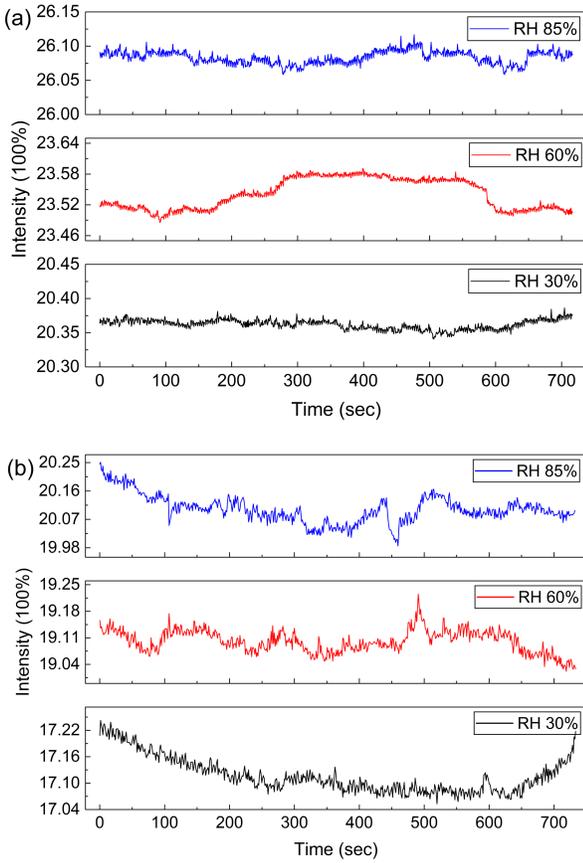
(a)

(b)

Fig. 7. Stability test of the proposed humidity sensor at fixed RH levels: (a) agarose-coated tapered twisted POF sensor, and (b) uncoated tapered twisted POF sensor.

Fig. 8. Real-time response of the proposed sensor to human breath.

exposure, pixel averaging, and imaging geometry. Despite this, the smartphone provides a dense, high-rate signal at video frame rates, helping capture fast variations in the coupled output and demonstrating its capability to reliably track rapid changes, reassuring the audience of its effectiveness for dynamic measurements. Notably, the fitted trends remain consistent in both humidification and dehumidification, indicating that the portable RH sensor maintains stable calibration across repeated RH cycling.

E. Portable Sensor Stability

To further assess the portable RH sensor, we conducted stability tests at fixed humidity setpoints of 30%, 60%, and 85% for a duration exceeding 700 s. As shown in Fig. 7(a), the agarose-coated sensor output remains essentially constant at each RH level, with only minor time-dependent variation. The signal is notably low-noise, and the fluctuations stay within approximately ±0.05% of the mean value, indicating negligible drift during extended operation. Fig. 7(b) shows the response of the uncoated tapered twisted POF under the same conditions, which exhibits larger fluctuations and more noticeable drift. This comparison confirms that the agarose coating improves the stability and repeatability of the portable sensor output, which is important for practical deployment where continuous monitoring requires consistent readings without
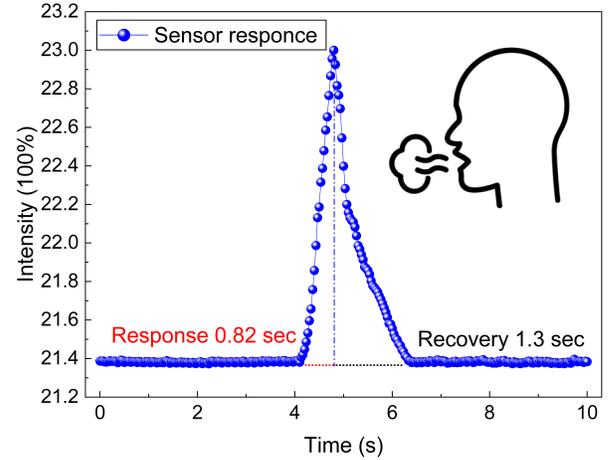
baseline shift. Taken together with the observed sensitivity, these results demonstrate that the smartphone-interrogated POF platform can deliver reliable humidity measurements over prolonged periods.

F. Response Time

We further evaluated the transient response of the portable agarose-coated RH sensor under typical indoor conditions ambient RH $\approx 45\%$ at 25°C. As shown in Fig. 8, the sensing region was briefly exposed to a short burst of human breath to introduce a rapid humidity change. The recorded optical intensity increased immediately upon contact with the humid airflow and then returned promptly to its baseline once the airflow stopped. The measured response time was 0.82 s, and the recovery time was 1.3 s, demonstrating the sensor's ability to track abrupt humidity fluctuations with minimal delay. This fast dynamic behavior is attributed to the agarose coating, which rapidly absorbs and releases moisture, enabling quick modulation of the local refractive index and, consequently, the coupled optical power.

Overall, the experimental results confirm that combining a tapered coupling structure with an agarose coating provides a simple and effective route to intensity-based RH sensing over a wide operating range. The power meter measurements establish the role of tapering in strengthening coupling and increasing humidity-dependent modulation. At the same time, the smartphone interrogation reproduces the same calibration trends with high linearity, demonstrating that reliable sensing can be achieved without laboratory-grade instrumentation. Taken together, these outcomes indicate that the proposed sensor is a practical candidate for real-time RH monitoring in applications that require a compact form factor, rapid response, and field-deployability.

IV. CONCLUSION

The present study successfully demonstrates the development and performance evaluation of a portable RH sensor based on POFs. The sensor fabrication incorporates a tapered twisted coupling structure that increases interaction

between the guided optical field and the surrounding medium, thereby improving side-coupling efficiency and strengthening the humidity-dependent intensity modulation. The active sensing region is formed by coating the tapered coupled zone with a thin agarose gel layer, which functions as a hygroscopic transduction element. As ambient humidity increases, water molecules are absorbed into the agarose network, causing the coating to swell and modify the local refractive-index boundary and coupling condition between the two fibers. This produces a measurable change in the coupled optical power, enabling RH detection through an intensity-modulation mechanism. To enable practical deployment outside the laboratory, the sensor was interrogated using a standard smartphone, where the flashlight served as the illumination source and the rear camera acted as the detector. The sensor exhibits a linear response over the 20% to 90% RH range and achieves sensitivities of. 0.117 μW/%RH using a laboratory power meter and 0.108 ± 0.005 %/%RH using the smartphone-based normalized intensity readout, with an RH resolution of approximately 0.12 ± 0.01% RH, confirming its capability to track rapid humidity variations in real time.

REFERENCES

[1] S. Kang, K. Zhao, D.-G. Yu, X. Zheng, and C. Huang, "Advances in biosensing and environmental monitoring based on electrospun nanofibers," *Advanced Fiber Materials*, vol. 4, no. 3, pp. 404–435, Jun. 2022.

[2] V. Kumar, S. K. Raghuwanshi, and S. Kumar, "Advances in nanocomposite thin-film-based optical fiber sensors for environmental health monitoring–A review," *IEEE Sensors Journal*, vol. 22, no. 15, pp. 14696-14707, 2022.

[3] Z. Duan, Y. Jiang, and H. Tai, "Recent advances in humidity sensors for human body related humidity detection," *Journal of Materials Chemistry C*, vol. 9, no. 42, pp. 14963–14980, 2021.

[4] M. A. Butt, G. S. Voronkov, E. P. Grakhova, R. V. Kutluyarov, N. L. Kazanskiy, and S. N. Khonina, "Environmental monitoring: A comprehensive review on optical waveguide and fiber-based sensors," *Biosensors*, vol. 12, no. 11, 2022.

[5] Y. Wang, C. Shen, W. Lou, and F. Shentu, "Polarization-dependent humidity sensor based on an in-fiber Mach–Zehnder interferometer coated with graphene oxide," *Sensors and Actuators B: Chemical*, vol. 234, pp. 503–509, Oct. 2016.

[6] R. D'Amato, A. Polimadei, G. Terranova, and M. A. Caponero, "Humidity sensing by chitosan-coated fibre Bragg gratings (FBG)," *Sensors*, vol. 21, no. 10, 2021.

[7] R. J. Tong, Y. Zhao, M.-Q. Chen, and Y. Peng, "Relative humidity sensor based on small up-tapered photonic crystal fiber Mach–Zehnder interferometer," *Sensors and Actuators A: Physical*, vol. 280, pp. 24–30, Sep. 2018.

[8] R.-J. Tong, Y. Zhao, H.-K. Zheng, and F. Xia, "Simultaneous measurement of temperature and relative humidity by compact Mach–Zehnder interferometer and Fabry–Perot interferometer," *Measurement*, vol. 155, p. 107499, Apr. 2020.

[9] T. Cheng *et al.*, "A surface plasmon resonance optical fiber sensor for simultaneous measurement of relative humidity and temperature," *IEEE Sensors Journal*, vol. 22, no. 4, pp. 3246–3253, 2022.

[10] Z. Ahmad, Q. Zafar, K. Sulaiman, R. Akram, and K. S. Karimov, "A humidity sensing organic-inorganic composite for environmental monitoring," *Sensors*, vol. 13, no. 3, pp. 3615–3624, 2013.

[11] N. Alam, Abid, and S. S. Islam, "Advancements in trace and low humidity sensors technologies using nanomaterials: A review," *ACS Applied Nano Materials*, vol. 7, no. 12, pp. 13836–13864, Jun. 2024.

[12] J. Y. Guo, B. Shi, M.-Y. Sun, C.-C. Zhang, G.-Q. Wei, and J. Liu, "Characterization of an ORMOCER®-coated FBG sensor for relative humidity sensing," *Measurement*, vol. 171, p. 108851, Feb. 2021.

[13] S. Zhang, B. Dong, Z. Chen, P. Lin, and W. Huang, "Pentaerythritol tetraacrylate microcavity sensor for high performance relative humidity detection," *Sensors and Actuators A: Physical*, vol. 366, p. 114981, Feb. 2024.

[14] M. Q. Chen, Y. Zhao, H. M. Wei, C.-L. Zhu, and S. Krishnaswamy, "3D printed castle style Fabry–Perot microcavity on optical fiber tip as a highly sensitive humidity sensor," *Sensors and Actuators B: Chemical*, vol. 328, p. 128981, Feb. 2021.

[15] S. H. Johari *et al.*, "ZnO nanorods coated tapered U-shape plastic optical fiber for relative humidity detection," *Photonics*, vol. 9, no. 11, 2022.

[16] J. Fu, Y. Xu, M. Xu, L. G. Abbas, and A. Zhou, "Highly sensitive humidity sensor based on tapered dual side-hole fiber," *Optik*, vol. 261, p. 169183, Jul. 2022.

[17] M. S. B. Sadeque *et al.*, "Hydrogel-integrated optical fiber sensors and their applications: a comprehensive review," *Journal of Materials Chemistry C*, vol. 11, no. 28, pp. 9383–9424, 2023.

[18] R. L. Xia *et al.*, "Compact fiber Fabry–Perot sensors filled with PNIPAM hydrogel for highly sensitive relative humidity measurement," *Measurement*, vol. 201, p. 111781, Sep. 2022.

[19] Y. Hu, A. Ghaffar, Y. Hou, W. Liu, F. Li, and J. Wang, "A micro structure POF relative humidity sensor modified with agarose based on surface plasmon resonance and evanescent wave loss," *Photonic Sensors*, vol. 11, no. 4, pp. 392–401, Dec. 2021.

[20] R. Tong, Y. Wang, K.-J. Zhao, X. Li, and Y. Zhao, "Surface plasmon resonance optical fiber sensor for relative humidity detection without temperature crosstalk," *Optics & Laser Technology*, vol. 150, p. 107951, Jun. 2022.

[21] Y. Wang, J. Wang, Y. Shao, C. Liao, and Y. Wang, "Highly sensitive surface plasmon resonance humidity sensor based on a polyvinyl-alcohol-coated polymer optical fiber," *Biosensors*, vol. 11, no. 11, 2021.

[22] S. Hussian *et al.*, "Development of a dual point humidity sensor using POF based on twisted fiber structure," *Scientific Reports*, vol. 14, no. 1, p. 10735, May 2024.

[23] A. Ghaffar *et al.*, "A low-cost relative humidity sensor using polymer optical fiber based on intensity variation," *IEEE Sensors Journal*, vol. 24, no. 6, pp. 7816–7823, 2024.

[24] A. Ghaffar *et al.*, "The design and validation of an intensity-modulated multipoint fiber-optic liquid-level sensor," *Sensors*, vol. 25, no. 16, 2025.

[25] C. Yang *et al.*, "Portable optical fiber biosensors integrated with smartphone: technologies, applications, and challenges [Invited]," *Biomedical Optics Express*, vol. 15, no. 3, pp. 1630–1650, Mar. 2024.

[26] L. Lu *et al.*, "A portable optical fiber SPR temperature sensor based on a smart-phone," *Optics Express*, vol. 27, no. 18, pp. 25420–25427, Sep. 2019.

[27] W. Z. Khan, Y. Xiang, M. Y. Aalsalem, and Q. Arshad, "Mobile phone sensing systems: a survey," *IEEE Communications Surveys & Tutorials*, vol. 15, no. 1, pp. 402–427, 2013.

[28] M. S. U. K. Haider *et al.*, "Portable optical fiber sensor for continuous liquid level sensing using commercially available POF," *IEEE Sensors Journal*, vol. 25, no. 3, pp. 4582–4589, 2025.

[29] M. S. U. K. Haider, C. Chen, A. Ghaffar, L. U. Noor, S. Hussain, and M. Liu, "High-resolution portable dual-point liquid level measurement system using POF," *Journal of Lightwave Technology*, vol. 43, no. 17, pp. 8443–8451, Sep. 2025.

[30] M. S. U. K. Haider *et al.*, "Smartphone-based optical fiber sensor for refractive index sensing using POF," *Sensors and Actuators A: Physical*, vol. 385, p. 116321, Apr. 2025.

[31] M. Batumalay, S. W. Harun, F. Ahmad, R. M. Nor, N. R. Zulkepely, and H. Ahmad, "Study of a fiber optic humidity sensor based on agarose gel," *Journal of Modern Optics*, vol. 61, no. 3, pp. 244–248, Feb. 2014.

[32] D. Marcuse, "Coupled power equations for backward waves," *IEEE Transactions on Microwave Theory and Techniques*, vol. 20, no. 8, pp. 541–546, 1972.

[33] D. Marcuse, "Derivation of coupled power equations," *Bell System Technical Journal*, vol. 51, no. 1, pp. 229–237, Jan. 1972.